Spectral responses in granular compaction

Ling-Nan Zou (邹岭楠)*
The James Franck Institute and Department of Physics, The University of Chicago, Chicago, Illinois 60637, USA
(Received 22 October 2009; published 30 March 2010)

The slow compaction of a tapped granular packing is reminiscent of the low-temperature dynamics glasses. Here, I study the dynamics of granular compaction by means of a volumetric spectroscopy. While the specific packing volume v displays glassy aging and memory effects at low tapping amplitudes Γ, the dynamic volumetric susceptibility $\tilde{\chi}_v = \partial v / \partial \Gamma$ displays minimal glassy effects, and its frequency spectrum gives no indication of a rapidly growing time scale. These features are contrast sharply with that found in the dielectric and magnetic susceptibilities of structural and spin glasses. Instead, $\tilde{\chi}_v$ appears to exhibit the behavior of a dynamic configurational specific heat, such as that obtained from computer simulations of spin-glass models. This suggests that the glassy dynamics of granular compaction is controlled by statistically rare processes that diverge from the typical dynamics of the system. From modifications of the dynamical spectrum by finite system size, I suggest that these glassy processes derive from large-scale collective particle rearrangements.

DOI: 10.1103/PhysRevE.81.031302 PACS number(s): 45.70.Cc, 64.70.P−

I. RANDOM PACKING AS A MODEL GLASS

Filling a container by pouring in spherical grains nearly always leads to a disordered packing. The "ground state" of the system, a face-centered cubic packing and the densest arrangement of spheres, is rarely achieved unless put in by hand. Shaking or tapping the container, causing the contents to settle and compact, works only so well: the packing remains disordered, and its packing density ρ approaches but does not exceed the random close packing (RCP) density $\rho_{\mathrm{rcp}} \approx 0.64$ [1–3]. Despite being a robustly reproducible structure, both experimentally and on the computer, we know little about the origins of RCP.

The detailed particle arrangements in RCP bear surprising similarities to the molecular arrangements in simple liquids [4–8]; but unlike a liquid, RCP is mechanically rigid and resists shear—it is jammed [9]. The same combination of rigidity and disorder also characterizes glassy solids; indeed, the structure of simple metallic glasses is well-modeled by RCP [10–12]. Drawing on these similarities, it was proposed that jammed packing of grains and glass formation in simple liquids may be united into a Jamming Phase Diagram spanned by inverse density $1/\rho$, temperature T, and shear stress (Fig. 1) [13]. The region of high ρ, low T, and small shear is occupied by jammed or glassy states; the rest are filled by fluid states. Jamming is the consolidation of loose grains into a rigid packing when ρ is increased at $T=0$, while the glass transition is the freezing of liquid into glass at some finite T. Recent studies suggest that this picture is applicable not only to spherical grains and small molecule liquids, but also to chains and polymers as well [14,15].

Here, I explore dynamical, rather than structural, similarities between jammed packings and glasses. I am motivated by the fact that granular packings can exhibit slow dynamics similar to that exhibited by structural glasses, and by "glassy" systems such as spin glasses and kinetically constrained glassy models [16–18]. For a glass-former such as glycerol, small reductions in T lead to large increases in the relaxation time and the fluid viscosity. Below the glass transition temperature T_g, the equilibration time of the liquid is greater than the experimental time scale: the liquid falls out of equilibrium, becoming a glass whose properties are not stationary but depend on experimental time scale (aging) and thermal history (memory). For a packing of grains with dissipative interactions (friction), thermal energy is unimportant, and dynamical evolution is driven by external driving (e.g., tapping or shaking). Strongly shaken, a packing quickly reaches a loose-packed steady state. Weakly tapped, the packing compacts slowly, and the steady state may not be accessible on experimental time scales (Fig. 2); furthermore, the detailed evolution will depend on how the packing was prepared [19–25].

I will therefore take the random packing of grains provisionally to be a "glass." This raises the question if the various "glassy" systems can be described by a common set of physical processes. Simply put: is a granular packing glassy in the same sense as a structural or spin glass? If the answer is "yes," then granular compaction may serve as a useful model for studying glassy dynamics. Here, I have developed a volumetric spectroscopy, modeled after the dielectric and

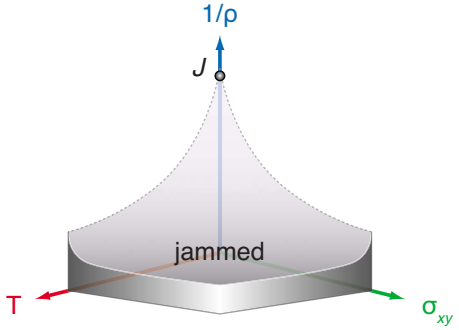

FIG. 1. (Color online) The Jamming Phase Diagram spanned by orthogonal axes inverse density $1/\rho$, temperature T, and shear stress σ_{xy}. The shaded volume is occupied by jammed or glassy states; the rest is filled by fluid states. Point J marks the $T=0$, $\rho=\rho_{\mathrm{rcp}}$ jamming transition.

*zou@uchicago.edu

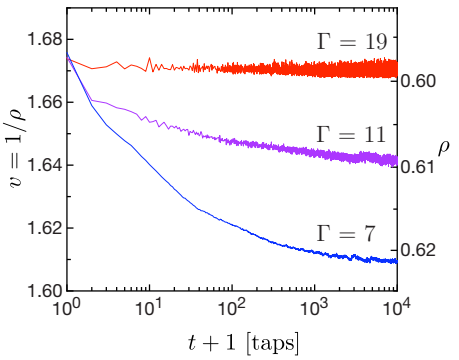

FIG. 2. (Color online) Granular compaction under steady tapping; $v \equiv 1/\rho$ is the specific packing volume, t is the number of taps applied, and Γ is the tapping amplitude (see Sec. II A). Strongly tapped (Γ large), the packing quickly reaches a steady state; weakly tapped (Γ small), the packing volume compacts slowly, and the steady state is not accessible within the experimental time scale.

magnetic spectroscopies of structural and spin glasses, to directly probe the dynamics of granular compaction. My goal is to make detailed comparisons between the dynamics of granular compaction with that of structural and spin glasses. Without a well-defined statistical mechanics for externally driven granular matter, analogies to glasses at finite T cannot be justified *a priori*. I will take a purely operational approach: analogies will be proposed naïvely, and justified only by the light they shed on experiments.

This paper is organized as follows:

Section II describes the volumetric spectroscopy and gives operational definition for the volumetric "susceptibility" $\tilde{\chi}_v$. I will then describe the experimental system in which this spectroscopy is realized.

Section III describes the behavior of $\tilde{\chi}_v$ as a function of the tapping amplitude Γ (which is the principal control parameter for granular compaction) and the frequency. Despite some similarities to the dielectric and magnetic susceptibilities of structural and spin glasses, $\tilde{\chi}_v$ is distinctive in exhibiting very weak glassy effects. More surprisingly, the spectrum of $\tilde{\chi}_v$ gives no indication of a diverging time scale as $\Gamma \to 0$.

In Sec. IV, I suggest $\tilde{\chi}_v$ may be interpreted as a dynamic configurational specific heat. The relationship between $\tilde{\chi}_v$ and specific volume fluctuation is found to be consistent with an effective Fluctuation-Dissipation Theorem (FDT), while computer simulations find the specific heat of standard spin-glass models behaves very similarly to $\tilde{\chi}_v$. These results suggest that the glassy dynamics of granular compaction is controlled by statistically rare processes that diverge from typical dynamics as Γ is reduced.

Section V describes how the system size modifies the dynamics of granular compaction. For small systems, $\tilde{\chi}_v$ is suppressed within an intermediate frequency band and within an intermediate window of tapping amplitude. Assuming $\tilde{\chi}_v$ to be a specific heat, this suggests the rare, low-frequency processes in granular compaction is due correlated particles motions over large length scales.

To conclude, in Sec. VI, I summarize the most salient results and briefly discuss their implications for understanding "glassy" dynamics. I will close by suggesting ways that this work can be extended to address some of the important open questions.

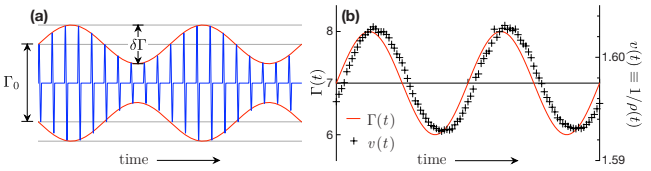

FIG. 3. (Color online) (a) Amplitude modulation of discrete taps. (b) Input: $\Gamma(t)$, amplitude-modulated tapping as a function of the tap number t (solid line). Experimentally measured response: frequency-locked modulation in the specific packing volume $v(t)$ (crosses). Note that $\Gamma(t)$ and $v(t)$ are slightly out of phase.

II. VOLUMETRIC SPECTROSCOPY OF GRANULAR COMPACTION

Experimentally, the dynamics of structural and spin glasses are frequently studied using some type of spectroscopy. There, temperature T is generally the principal control parameter that determines if the system is in the glassy state. Having set T, the system dynamics is characterized by some dynamic susceptibility describing how the system responds to small perturbations. For example, the dielectric susceptibility ϵ describes the how the net polarization $\mathbf{P}$ responds to a small applied electric field $\mathbf{E}$: $\epsilon = \partial \mathbf{P}/\partial \mathbf{E}$. By applying an oscillatory perturbation, e.g., an ac electric field, one can measure a frequency spectrum of dynamical responses on various time scales. Here, I will probe the dynamics of granular compaction using the response of the specific packing volume $v \equiv 1/\rho$ to small changes in the external driving.

A. Operational definition

In typical compaction experiments, a granular packing (held inside a container) is compacted with a sequence of discrete taps, separated sufficiently apart so that the packing comes to rest before being tapped gain. Each tap is a single period of sinusoidal (30 Hz in my case) vertical vibration, and the tapping amplitude Γ is given by the peak-to-peak acceleration a_{pp} of the tap, normalized by $g = 9.8\ \mathrm{m/s^2}$: $\Gamma \equiv a_{\mathrm{pp}}/g$. To measure a susceptibility, the packing must be perturbed at the same time it is being tapped; however, we lack an easily accessible "field," which can couple to the system.

My solution is to use tapping both as the principal control parameter, and as the perturbing field. Instead of a sequence of identical taps, I modulate the tapping amplitude about a mean level [Fig. 3(a)],

$$\Gamma(t) = \Gamma_0 + \delta\Gamma \sin(2\pi f t). \tag{1}$$

The mean amplitude Γ_0 remains the principal control parameter, while the modulation amplitude $\delta\Gamma$ serves as the perturbation; here f is the modulation frequency in inverse taps, and t is time measured in the number of taps. In response to the modulated tapping, the temporal evolution of the specific packing volume $v \equiv 1/\rho$ can be described as the sum of a

slowly varying component v_0, and a frequency-locked component which is phase-shifted with respect to the input [Fig. 3(b)],

$$v(t) \approx v_0 + \delta v \sin(2\pi f t - \varphi). \tag{2}$$

Here δv is the response magnitude, and φ is the phase shift between "excitation" (modulated tapping) and volumetric response. The real and imaginary parts of a dynamic volumetric susceptibility $\tilde{\chi}_v = (\chi_v', \chi_v'')$ are then

$$\chi_v' = \left(\frac{\delta v}{\delta \Gamma}\right)\cos\varphi, \quad \chi_v'' = \left(\frac{\delta v}{\delta \Gamma}\right)\sin\varphi. \tag{3}$$

Here, $\tilde{\chi}_v$ describes how v responds to a small change in the tapping amplitude. For weak perturbations, the response should be linear, $\delta v \propto \delta\Gamma$, and $\tilde{\chi}_v$ should be independent of the modulation amplitude.

In practice, φ and δv are not directly extracted from $v(t)$. Using the orthonormality of trigonometric functions, $\tilde{\chi}_v$ can be directly extracted by projecting $v(t)$ onto its in- and out-of-phase components (with respect to the tapping modulation). Once a $v(t)$ time series is collected, it is divided into time-blocks of length $1/f$, synchronized to the tapping modulation. Within each time-block, $v(t)$ is discretely transformed to extract $\tilde{\chi}_v$

$$\chi_v'(t) = \frac{2f}{\delta\Gamma}\sum_{\tau=0}^{1/f-1} v(t+\tau)\sin(2\pi f\tau), \tag{4}$$

$$\chi_v''(t) = \frac{2f}{\delta\Gamma}\sum_{\tau=0}^{1/f-1} v(t+\tau)\sin(2\pi f\tau - \pi/2). \tag{5}$$

Formally, Eqs. (4) and (5) are exact only if the background v_0 is stationary. However, so long as v_0 is slowly varying on the time scale of $1/f$, Eqs. (4) and (5) are good approximations.

B. Experimental design

The experimental design here is modeled after that of [19]. I use a tall cylindrical packing in order to suppress large-scale convections during the compaction process. The container cell is a smooth-walled polycarbonate cylinder, 50 cm tall, with an inner diameter $D=2.5$ cm. To minimize static buildup, the inside cell wall is coated with a hard conductive polymer coating (Agfa Orgacon S103). For experiments, the cell is filled with particles to a height of ≈ 40 cm [Fig. 4(a)] and mounted on a computer-controlled electromechanical shake set on a vibration-damped platform. To reduce unwanted lateral motions during tapping, the cell is braced to a stiff external framework with heavy-duty elastic bands.

The particles used are spherical zirconium oxide/silica ceramic (material density=3.88 g/cm^3) particles (Glenn Mills), which are mechanically tougher than glass beads and have a much smoother surface. This reduces abrasion on the cell and on the particles themselves, helping to ensure good reproducibility over the course of long experiments and millions of taps. Particles of three different diameters were used:

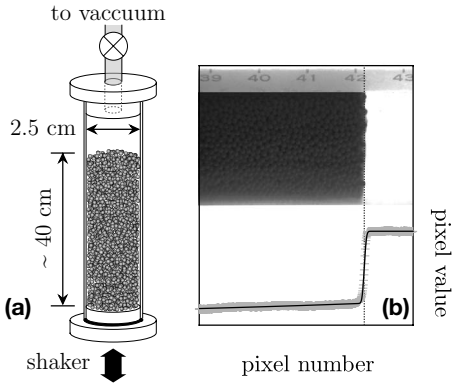

FIG. 4. (a) The experimental setup used to measure $\tilde{\chi}_v$ (schematic not drawn to scale). (b) A photograph of the packing; its image profile is fitted to extract the packing height, and hence the specific packing volume v.

$d=0.5$ mm, 1.1 mm, and 1.8 mm, all with $\sim 10\%$ polydispersity. Since air effects can strongly alter the compaction process [26], once loaded, the cell is sealed and evacuated to a pressure <5 Pa.

To measure the packing volume, a photograph of the packing is taken after each tap, using a computer-controlled digital camera running Astro IIDC (Outcast Software). The cell is uniformly backlit: where the cell is filled with grains, the image is dark. Fitting the image intensity profile to an error function, I locate the top surface of the packing [Fig. 4(b)]. This is compared with reference marks on the cell to extract the packing height and volume. The absolute accuracy in measuring v is limited by unevenness of the top surface, and by the accuracy with which reference marks are placed. These are compensated by a large fill height, which keeps the absolute uncertainty in v to $\sim 5\times 10^{-3}$. The relative accuracy, most important for our purposes, is $\sim 10^{-4}$ since image profiles are fitted with subpixel resolution.

To reset the system at the start of each new experimental trial, the packing is tapped at $\Gamma=21$ for at least 10^3 taps. The result is a reproducible loose packing with steady-state dynamics, where all memory of its prior tapping history is lost.

III. VOLUMETRIC RESPONSE

The volumetric susceptibility $\tilde{\chi}_v$ depends on both Γ_0, which is the principal control parameter, and the modulation frequency f. It should not depend on $\delta\Gamma$ if the response is linear, $\delta v \propto \delta\Gamma$. At low Γ_0, where granular compaction exhibits glassy behavior, $\tilde{\chi}_v$ should in principle depend on both the experimental time scale (aging) and the history of the packing (memory). Indeed this is what we expect based on the behavior of dielectric and magnetic susceptibilities in structural and spin glasses. (All results in this Section were obtained with $d=0.5$ mm particles, giving an effective system size of $D/d=50$.)

A. Dependence of $\tilde{\chi}_v$ on Γ_0 and $\delta\Gamma$

Figure 5 plots $\tilde{\chi}_v$ as a function of Γ_0, for different modulation frequencies f, with $\delta\Gamma=1$. Here, Γ_0 is ramped from

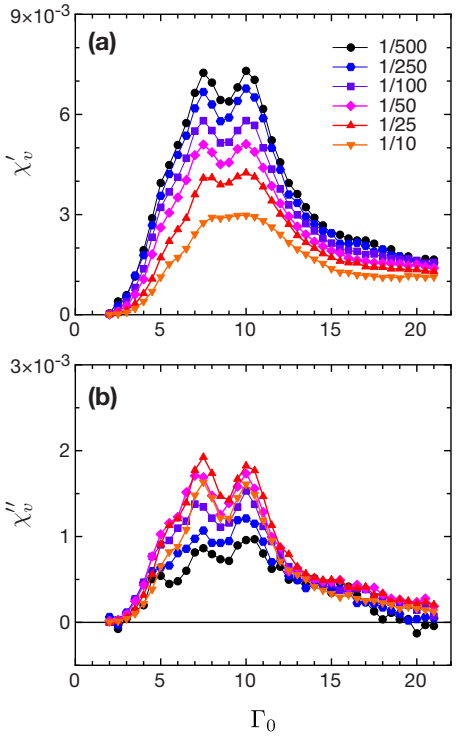

FIG. 5. (Color online) The (a) real and (b) imaginary parts of the volumetric susceptibility $\tilde{\chi}_v$ as a function of Γ_0, measured at different modulation frequencies f.

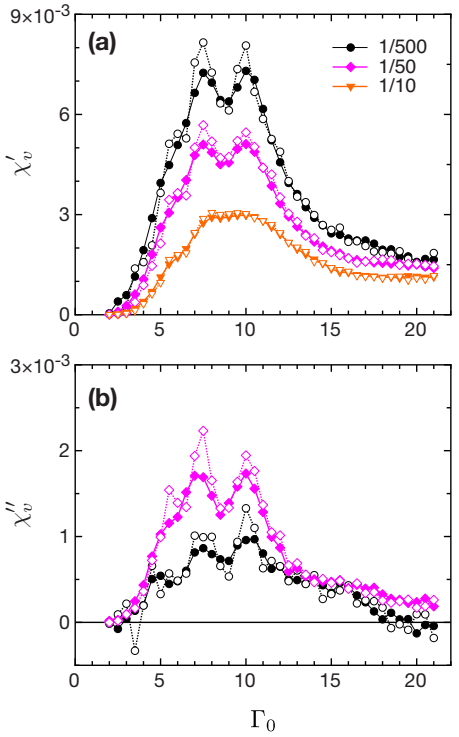

FIG. 6. (Color online) Testing for linear response: (a) χ_v' and (b) χ_v'' measured using $\delta\Gamma=1$ (filled symbols) and $\delta\Gamma=0.5$ (open symbols) at several different frequencies. The similarity of the resulting curves shows the experiment is in the linear response regime.

$\Gamma_0=21$ to $\Gamma_0=2$ and cycled back in steps of $\Delta\Gamma_0=0.5$ and a dwell time $\tau_{\rm dw}=500$ taps per step. Each data point represents the average of all measurements taken within the dwell time (i.e., for $f=1/50$, 10 measurements of $\tilde{\chi}_v$ were made at each Γ_0 point). As a function of Γ_0, both χ_v' and χ_v'' exhibit a broad maximum centered near $\Gamma_0\approx 8$ for all frequencies measured. The broad maximum is structured, with subpeaks (found in both χ_v' and χ_v'') at $\Gamma_0=10$ and $\Gamma_0=7.5$, and a "knee" at $\Gamma_0=5$. At low frequencies, the real response is stronger, and the fine features in $\chi_v'(\Gamma_0)$ are more prominent; on the other hand, the imaginary response is weakened.

As Γ_0 and T are, respectively, the principal control parameters for granular compaction and for glass formation, it is reasonable to compare $\tilde{\chi}_v(\Gamma_0)$ with the T-dependent susceptibilities of glasses. Qualitatively, $\tilde{\chi}_v(\Gamma_0)$ has broad similarities to the magnetic susceptibility $\tilde{\chi}_M(T)$ of spin glasses, such as CuMn, as well as the dielectric susceptibility $\tilde{\epsilon}(T)$ of structural glasses such as glycerol [27,30,31]. However, for most structural and spin glasses, the peak in $\tilde{\epsilon}(T)$ or $\tilde{\chi}_M(T)$ is simple in structure, whereas $\tilde{\chi}_v(\Gamma_0)$ exhibits multiple subpeaks. For glasses, the peak in $\tilde{\epsilon}(T)$ or $\tilde{\chi}_M(T)$ shifts to lower T for lower frequencies. In granular compaction, the fine features $\tilde{\chi}_v(\Gamma_0)$ remains at the same values of Γ_0.

Figure 6 compares $\tilde{\chi}_v(\Gamma_0)$ measured with $\delta\Gamma=1$ to that with $\delta\Gamma=0.5$: the two results are nearly identical. This indicates the volumetric response is mostly linear within the range of f and Γ_0 probed. Closely examined, the subfeatures in $\tilde{\chi}_v(\Gamma_0)$ are more pronounced for smaller $\delta\Gamma$. This suggests the subpeaks of $\tilde{\chi}_v$ mark values of Γ_0 where volumetric response is most sensitive and most nonlinear; this is reminiscent of the sensitivity of systems perched near critical points.

A similar effect is found in spin glasses, where low field measurements yield larger, sharper peaks in the magnetic susceptibility. However, in spin glasses, the peak of $\tilde{\chi}_M$ shifts to higher T when measured using smaller fields [32,33], while in granular compaction the subpeaks of $\tilde{\chi}_v$ do not shift with $\delta\Gamma$.

For structural and spin glasses, the peak in the dielectric or magnetic susceptibility is often taken to mark the glass transition temperature T_g. Here, we can ask if the features of $\tilde{\chi}_v$ correspond to transitions in compaction dynamics. One candidate for such a transition is the branch point Γ^*, where the so-called reversible and irreversible branches of $v(\Gamma_0)$ converge [20]. For $\Gamma_0>\Gamma^*$, $v(\Gamma_0)$ is single-valued, and the packing reaches a steady state on the experimental time scale. For $\Gamma_0<\Gamma^*$, $v(\Gamma_0)$ can take any value in the region bounded by the reversible and irreversible branches, depending on the precise history of the packing [20,25]. Thus, Γ^* is akin to T_g in that for $T<T_g$, the properties of a glass depends on its thermal history (Fig. 7). As the convergence of the two branches is gradual, Γ^* is a not precise transition but depends (weakly) on the ramping rate of Γ_0. This is reminiscent of the weak cooling rate dependence of T_g in glasses. Operationally, the volumetric susceptibility $\tilde{\chi}_v(\Gamma_0)$ is the dynamic "derivative" of the reversible branch of the compaction curve $v(\Gamma_0)$; thus the broadly peaked form of $\tilde{\chi}_v(\Gamma_0)$ is unsurprising. The subpeak in $\tilde{\chi}_v$ at $\Gamma_0=10$ is located near, but slightly below Γ^*. However, no outstanding feature in $v(\Gamma_0)$ corresponds to the equally prominent subpeak at $\Gamma_0=7.5$.

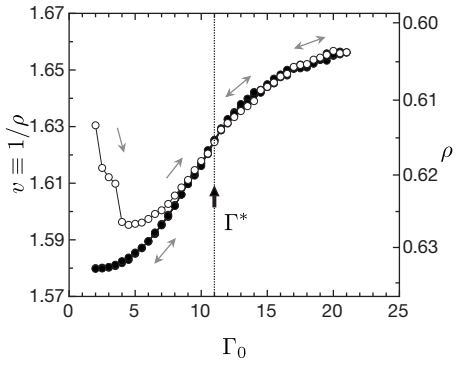

FIG. 7. The volumetric curve $v(\Gamma_0)$, showing the irreversible (open symbols) and reversible (filled symbols) branches. Arrows indicate the direction Γ_0 is ramped, and Γ^* marks where the two branches appears to converge.

B. Aging and memory effects in $\tilde{\chi}_v$

Figure 8(a) shows the behavior of granular compaction following a stepwise shift in Γ_0, starting from a loose-packed initial state. With the initial onset of tapping at $\Gamma_0=7$, v exhibits a strong aging signature and slowly compacts in a quasilogarithmic fashion with t. After 10^4 taps, Γ_0 is shifted down to $\Gamma_0=5$, and the system responds with a renewed bout of aging, relaxing to a smaller v. After 10^4 taps at $\Gamma_0=5$, Γ_0 is returned to $\Gamma_0=7$, whereupon the packing dilates to a v close to what it had just before the excursion to $\Gamma_0=5$. When the two $\Gamma_0=7$ portions of the $v(t)$ data are stitched together, the result is identical (aside from a transient) to an uninterrupted $\Gamma_0=7$ aging curve.

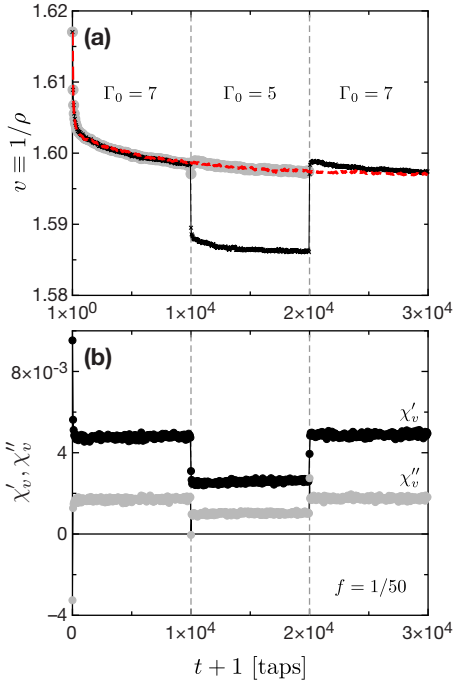

FIG. 8. (Color online) Granular compaction subjected to an stepwise shift protocol $\Gamma_0=7\rightarrow5\rightarrow7$, starting from a loose-packed initial state. (a) Specific volume $v(t)$ (crosses), showing strong aging signatures both initially, and at the negative shift to $\Gamma_0=5$. When the two $\Gamma_0=7$ portions of $v(t)$ stitched together (gray-filled circles), the results is the same as an uninterrupted $\Gamma_0=7$ $v(t)$ reference curve (bold broken line), aside from a brief transient. (b) The volumetric susceptibility $\tilde{\chi}_v$ measured in the same experiment. The aging signature is very weak, and the memory effect is trivial.

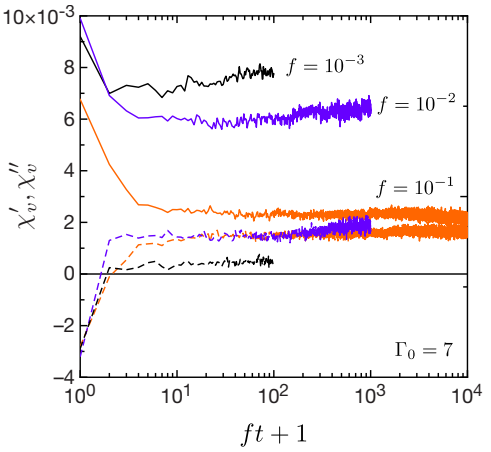

FIG. 9. (Color online) The relaxation of χ'_v (solid lines), χ''_v (broken lines) at $\Gamma_0=7$ for $f=10^{-1}$, 100^{-1}, and 1000^{-1} taps^{-1}; relaxation is mostly complete after $\sim 1/f$ taps.

In structural and spin glasses, this experiment is carried out via temperature shifts, and the aging and memory effects are observed in the dielectric or spin susceptibility [34,35]. It is a classic demonstration of both effects in a glassy system. For granular compaction, in the same experiment where aging and memory effects are clearly displayed in v, the volumetric susceptibility $\tilde{\chi}_v$ exhibits no discernible aging and memory signatures: $\tilde{\chi}_v$ relaxes within a few modulation periods $1/f$ to apparently static values in response to shifts of Γ_0 [Fig. 8(b)]. Figure 9 plots the relaxation of $\tilde{\chi}_v$ at $\Gamma_0=7$ for different frequencies: the system appears to be largely relaxed after a time scale on the order of $1/f$. The behavior $\tilde{\chi}_v$ can hardly be described as glassy, and is rather unlike that of the dielectric and magnetic susceptibilities of structural and spin glasses with their strong aging effects.

C. Spectrum of $\tilde{\chi}_v$

The weak aging of $\tilde{\chi}_v$ can be used to our advantage in the measurement of its spectrum. Even if the system is not in steady state, the measured $\tilde{\chi}_v$ should nevertheless be close to the "true" steady-state value. Thus the spectrum of $\tilde{\chi}_v$ can be measured down low Γ_0 where the steady state is experimentally inaccessible, with the confidence that the measured spectrum will be close to the steady-state one. Here, starting from a loosely packed initial state, Γ is slowly ramped stepwise (step size $\Delta\Gamma=0.5$, dwell time/step $\tau_{\rm dw}=500$ taps) to the working Γ_0. The packing is then tapped at the working Γ_0 (without modulation) until either steady state is achieved, or until the volumetric evolution is slow on the order of the lowest frequency to be probed. The amplitude modulation ($\delta\Gamma=1$) is then turned on, and the frequency swept from high frequencies to low.

Figure 10 plots the spectrum of $\tilde{\chi}_v(f)$ obtained for various values of Γ_0. Here, the spectrum of $\chi''_v(f)$ gives the

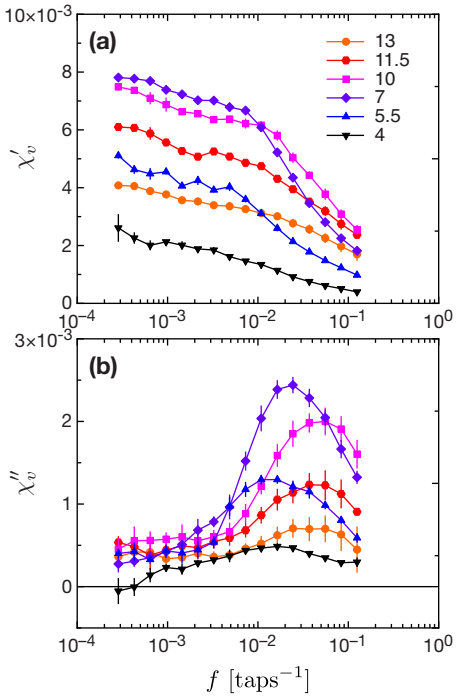

FIG. 10. (Color online) The (a) real and (b) imaginary parts of the $\tilde{\chi}_v$ spectrum, obtained at different values of Γ_0.

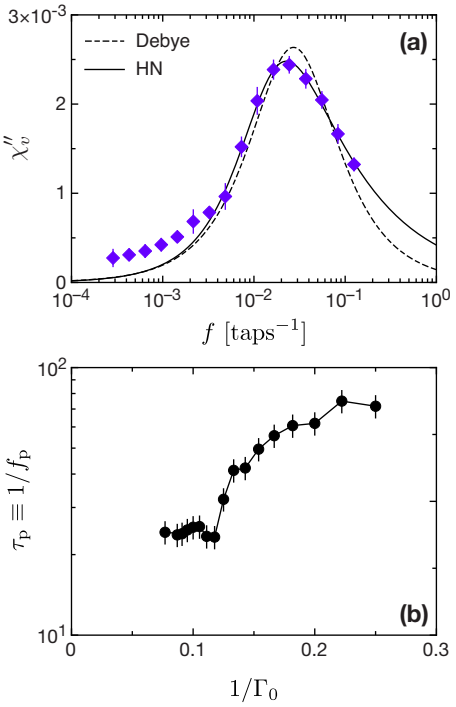

FIG. 11. (Color online) (a) The spectral peak in χ_v'' at $\Gamma_0=7$. Lines are fits to the spectral peak using Debye (broken line) and Havriliak-Negami (solid line) forms. (b) The characteristic relaxation time $\tau_p=1/f_p$ plotted against $1/\Gamma_0$.

frequency-distribution of dynamical processes in granular compaction. In overall form, the spectrum of $\tilde{\chi}_v$ is similar to its dielectric and magnetic counterparts in glasses, including a peaked imaginary part. As with glasses, the spectral peak in χ_v'' is wider than the Debye peak. In the vicinity of the peak frequency, χ_v'' it can be fitted to the generalized Havriliak-Negami form [36]

$$\tilde{\chi}_v(f) = \tilde{\chi}_v^{\infty} + \frac{\tilde{\chi}_v^0 - \tilde{\chi}_v^{\infty}}{[1 + (i2\pi f\tau)^{\alpha}]^{\beta}}, \tag{6}$$

with $\alpha \approx 1$ and $\beta \approx 0.5$ ($\alpha=\beta=1$ gives the Debye form) [Fig. 11(a)]; however, the low-f wing of χ_v'' is more that what a generalized, single-peak form [such as Eq. (6)] can account. For very small Γ_0, the volumetric response of $v(t)$ can be anharmonic. This can lead to low-f anomalies in the $\tilde{\chi}_v$ spectrum at small Γ_0, such as negative χ_v''s.

While the spectral peak in $\chi_v''(f)$ varies in height and shape with Γ_0, its location is nearly stationary. This is in sharp contrast to the dielectric and magnetic spectra of glasses, where a small reduction in T can shift spectral peaks to dramatically lower frequencies [27–29]. By fitting the peak in $\chi_v''(f)$ to Eq. (6), the peak frequency f_p (and equivalently, a characteristic dynamic time scale $\tau_p \equiv 1/f_p$) can be extracted. Figure 11(b) plots the inverse peak frequency $1/f_p \equiv \tau_p$ versus $1/\Gamma_0$. For $\Gamma_0 > 7.5$, $\tau_p \approx 25$ taps does not change with Γ_0; below $\Gamma_0=7.5$, τ_p grows modestly from $\tau_p \approx 25$ to 75 taps, and appears to saturate for very low Γ_0. There is no indication in the spectrum of χ_v'' that τ_p diverges as $\Gamma_0 \to 0$.

A characteristic relaxation time $\tau_p \approx 25-75$ taps can only be described as remarkably short. Even at the largest Γ_0 within this range, an loose-packed initial state will take thousands of taps to reach a steady state. Below $\Gamma_0 \approx \Gamma^* \approx 11.5$, when the steady state is practically inaccessible, τ_p as extracted from $\chi_v''(f)$ is at least 3 orders of magnitude smaller than the time it takes for a loose-packed initial state reach the steady state. The weak dependence of τ_p on Γ_0 in granular compaction is in sharp contrast to the behavior of glasses, where the inverse peak frequency of the dielectric and magnetic susceptibilities diverge as $\tau_p \sim e^{1/T}$ or even faster.

D. Anomalous "susceptibility"

The dependence of $\tilde{\chi}_v$ on Γ_0 and f, insofar as it describes the responses of a system with "glassy" dynamics, is rather anomalous. The weakness of its aging behavior, as well as the absence of a diverging time scale in its spectrum, places $\tilde{\chi}_v$ in sharp contrast to the familiar dielectric and magnetic susceptibilities of structural and spin glasses. Strangely, $\tilde{\chi}_v$ does not appear to capture the glassy dynamics of granular compaction: there is a broad separation between the characteristic time scale extracted from the dynamical spectrum, and the time scale a loose-packed initial state takes to arrive at steady state.

It may be that the anomalous behavior of $\tilde{\chi}_v$ is unique to granular compaction. In thermal systems, a susceptibility is defined as the response of a macroscopic thermodynamic observable with respect to its conjugate field, e.g., $\chi_M = \partial M/\partial h$. For granular compaction, where a well-defined statistical mechanics is absent, no principle dictates $\tilde{\chi}_v$ should be the analog of any thermodynamic susceptibility. But as I will suggest in Sec. IV, $\tilde{\chi}_v$ may not be so anomalous after all; rather, its behavior may represent that of the configurational specific heat.

IV. $\tilde{\chi}_v$ AS "SPECIFIC HEAT"

Granular compaction is an athermal system with strongly dissipative dynamics. However, tapping in granular compaction is akin to thermal excitation in that tapping activates transitions from one static configuration of particles to another, allowing the system to explore configuration space. Additionally, tapping amplitude Γ_0 controls whether compaction dynamics is glassy, analogous to the role T plays for glass dynamics.

Therefore, I propose the following analogy: take Γ_0 as the analog of T, with v playing the role of energy density [37,38], then $\tilde{\chi}_v$ should be thought as the dynamic configurational "specific heat" of granular compaction. As I will show, this naïve analogy proves to be very helpful toward understanding the experimental results.

A. Connection to specific volume fluctuations

In thermal equilibrium, the specific heat describes energy (or equivalently, entropy) fluctuations via the Fluctuation-Dissipation Theorem. Even though it is not an equilibrium thermal process, it remains reasonable to suppose that granular compaction system does not distinguish between spontaneous fluctuations and those induced by a small external perturbation, particularly in the linear response regime [39]. If $\tilde{\chi}_v$ is a "specific heat," then $\tilde{\chi}_v$ should describe steady-state volume fluctuation in granular compaction. Modeling after the FDT between specific heat and energy fluctuations [40,41], I hypothesize the steady state of granular compaction can be described by an effective FDT

$$S(f) = T_{\text{eff}}^2 \chi_v''(f)/f, \tag{7}$$

where $S(f)$ is the power spectrum of specific volume fluctuations and $T_{\text{eff}}=T_{\text{eff}}(f,\Gamma_0)$ is some effective temperature. In the simplest case, in exact analogy to FDT, T_{eff} should be frequency-independent for $f \ll 1/\tau_0$, where $\tau_0 \sim 1$ tap is a microscopic time scale.

As steady-state fluctuations in granular compaction are only accessible for large Γ_0, where χ_v'' is small and subject to large uncertainties, the range of Γ_0 over which Eq. (7) can be tested is narrow. Within this limitation, I independently measured steady-state specific volume fluctuations and the susceptibility spectrum $\tilde{\chi}_v(f)$ at $\Gamma_0=11.5$. Figure 12 plots the power spectrum $S(f)$ of specific volume fluctuations, and overplotted is the combination $\chi_v''(f)/f$. While $S(f)$ and $\chi_v''(f)/f$ are distinct at very high frequencies, they are roughly consistent with each other at lower frequencies over approximately two decades. This suggests away from the highest frequencies, the relationship between $\tilde{\chi}_v$ and specific volume fluctuations is consistent with that of an effective FDT. The high-frequency discrepancy may represent an unavoidable departure as $f \to 1$ taps^{-1}.

B. Comparison with glass-forming liquids

The dynamic specific heat (at constant pressure) $\tilde{c}_p = (c_p', c_p'')$ has been measured experimentally for a number of glass-forming liquids [42–45]. Approaching T_g from above, the real part $c_p'(T)$ is nearly flat until close to T_g, when it drops to a lower value over a relatively small span in temperature. Accompanying the steplike drop in $c_p'(T)$, the imaginary part $c_p''(T)$ grows from zero far above T_g to a peak centered at T_g, before decaying to zero with further cooling. The spectral evolution of $\tilde{c}_p$ with T shows a peak frequency in $c_p''(f)$ that shifts rapidly to lower f (indicative of ever larger relaxation times) as $T \to T_g$ from above. Qualitatively, the dynamic specific heat $\tilde{c}_p(f)$ of glass-forming liquids behave more similarly to dielectric or magnetic susceptibilities, rather than the volumetric susceptibility of granular compaction.

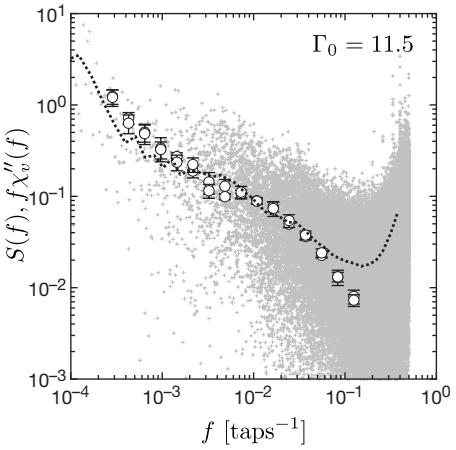

FIG. 12. Testing the effective FDT relationship between volume fluctuations and the volumetric susceptibility at $\Gamma_0=11.5$. Plotted are the power spectrum of steady-state volume fluctuations $S(f)$ (small crosses), $S(f)$ smoothed by averaging over logarithmically spaced bins (dotted line), and the combination $\chi_v''(f)/f$ (open symbols).

It is possible there exists a low-frequency band in the spectrum of $\tilde{\chi}_v$, outside of my experimental window, which does slow down as $\Gamma_0 \to 0$. This low-f band could then be analogous to the spectral features observed in the dynamic specific heat of liquids. In a molecular dynamics study of liquid SiO_2 approaching T_g from above, Scheidler *et al.* [46] found that the spectrum of the constant-volume specific heat $c_v''(f)$ possesses both a high-f band, which is stationary with T, and a low-f band which shifts to lower f as T decreases. There, the high-f band comes from the vibrational motion of molecules about a metastable configuration, while the low-f band is contributed by configurational rearrangements. It may be that the spectral features observed in granular compaction are analogous to the high-f band of vibrational processes. But as granular compaction is an athermal system with zero kinetic energy, this analogy unlikely to be appropriate.

C. Comparison with spin-glass models

A crucial distinction between glass-forming liquids and granular compaction is in the nature of their entropies. For a glass-forming liquid, entropy has both configurational contributions (from the spatial arrangement of molecules) and dynamic contributions (from the kinetic motion of molecules). For granular compaction, its entropy is purely configura-

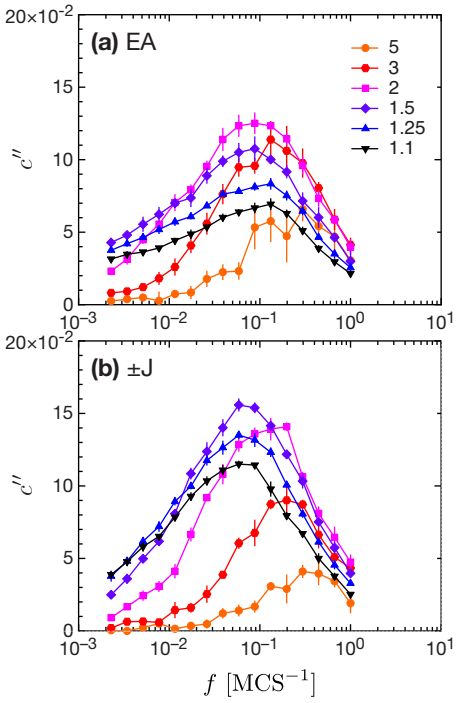

FIG. 13. (Color online) The imaginary part (c'') of the spin-glass specific heat $\tilde{c}$ spectrum, obtained at different temperatures T for (a) the Edwards-Anderson (EA) model, (b) the $\pm J$ model. Time is measured in Monte Carlo steps (MCS); 1 MCS=256 spin flip attempts.

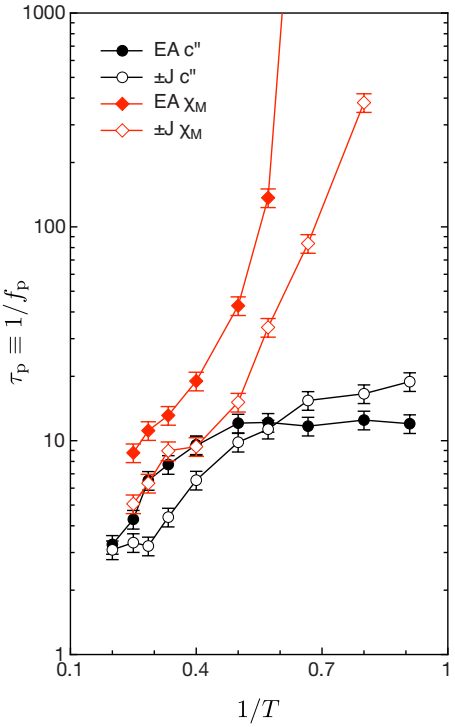

FIG. 14. (Color online) The characteristic energy relaxation time $\tau_p=1/f_p$, where f_p is the peak frequency in $c''(f)$, for the EA and $\pm J$ models (circles). Also shown are magnetic relaxation times obtained from the magnetic susceptibility spectrum for the same models (diamonds). As T is decreased, there is a rapidly growing separation of time scale between the specific heat and the magnetic susceptibility.

tional. Because specific heat is intimately connected to energy and entropy, this difference between glassy-forming liquids and granular compaction may prove crucial. Therefore, it may be more appropriate to compare $\tilde{\chi}_v$ with the specific heat of purely configurational systems, such as spin glasses.

The dc magnetic specific heat $c_{\rm mag}$ has been measured for several spin-glass systems. These have found $c_{\rm mag}(T)$ take broadly peaked forms, similar to $\tilde{\chi}_v(\Gamma_0)$, and in some cases exhibit subpeaks and knees [47–49]. However, such dc measurements gives no information about the dynamical processes involved.

In the absence of comparable experimental measurements on physical spin glasses, I used Monte Carlo computer simulations to study the dynamic specific heat $\tilde{c}=(c',c'')$ in two standard spin-glass models. I examined two-dimensional (2D) Ising models governed by the Hamiltonian

$$H=\sum_{(i,j)} J_{ij}S_iS_j - h\sum_i S_i \equiv H_0 - hM, \tag{8}$$

where $S_i=\pm 1$ are Ising spins occupying the sites of a 16 $\times$16 square lattice with periodic boundary conditions. Here h is an externally applied magnetic field, and J_{ij} are quenched random couplings between nearest neighbor spin pairs (i,j). For the Edwards-Anderson (EA) model, $\{J_{ij}\}$ are distributed in two unit-variance Gaussians centered at $J=\pm 1$; for the $\pm J$ model, J_{ij} takes on values of $\{-1,1\}$ with equal probability.

Figure 13 plots the spectrum of the imaginary specific heat $c''(f)$ obtained at different T for both the EA and $\pm J$ models. For both, the height and the shape of the spectral peak varies with T, but the inverse peak frequency $1/f_p \equiv \tau_p$ grows only modestly. (A similar effect has also been observed in small, randomly coupled Ising clusters on a triangular lattice [50].) The qualitative behavior is surprisingly similar to that of the volumetric response of granular compaction (Fig. 14). I have also found that at low T, $\tilde{c}$ shows much weaker aging effect than both the overall energy H and the magnetic susceptibility $\tilde{\chi}_M$, reminiscent of the weak aging signature in $\tilde{\chi}_v$. Thus the apparently distinctive features of $\tilde{\chi}_v$—weak aging effects and the absence of a diverging time scale—also seems to characterize the dynamic configurational specific heat of spin glasses.

D. Rare events control glassy behavior?

Like $\tilde{\chi}_v$, the dynamic specific heats of the spin-glass models studied here are characterized by short characteristic time scales and weak glassy effects. On the other hand, the magnetic susceptibility in the same models do exhibit rapidly diverging time scales as $T\to 0$ (Fig. 14). This shows for spin glasses, on cooling, there is a rapid separation of time scales between characteristic energy/entropy fluctuations, which remain fast, and magnetic fluctuations, which slow down and give rise to glassy behavior. Since all dynamical processes, including magnetic fluctuations, must contribute to the spe-

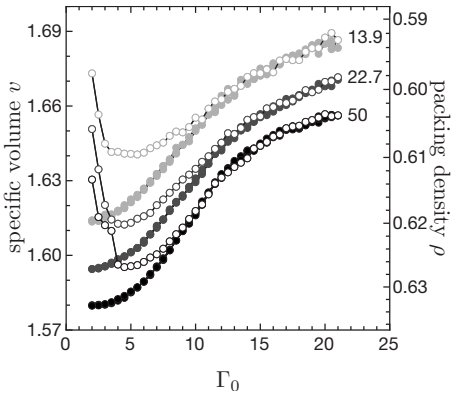

FIG. 15. The compaction curve $v(\Gamma_0)$, showing both irreversible (open symbols) and reversible branches (filled symbols), obtained for packings with $D/d=50$, 22.7, and 13.9. The ramping of Γ_0 is in steps of $\Delta\Gamma_0=0.5$, $\tau_{dw}=500$ taps.

cific heat, that the specific heat spectrum gives no indication of glassiness suggests that the low-f processes responsible for glassy behavior have little statistical weight.

Is a similar effect at work in granular compaction? If $\tilde{\chi}_v$ is analogous to the specific heat, it should capture all the dynamics of granular compaction. That we see no indication of a diverging dynamical time scale in χ_v'' suggests glassy dynamics in granular compaction are controlled by statistically rare processes in the low-frequency wing that become separated from typical volumetric processes as Γ_0 is reduced, leading eventually to broken ergodicity [51,52]. But what is the nature of these rare, low-frequency dynamical processes? Analyses of finite-size modifications to the volumetric response suggest that these glassy processes arise from the collective rearrangement of particles over extended length scales.

V. FINITE-SIZE EFFECTS

If $\tilde{\chi}_v$ is a specific heat analog, then it should be an intensive quantity independent of the system size. However, for a system confined with one or more very small dimensions, its behavior can become qualitatively different and sensitive to system size. Most obviously, the properties of a small system with large surface-to-volume ratio will be dominated by the surface rather than the bulk. More subtly, if collective processes contribute significantly to system dynamics, then the specific heat of a small system may be suppressed by the truncation of large-scale collective processes.

A. Rescaling the system: the effect on v and $\tilde{\chi}_v$

By packing particles of diameters $d=0.5$, 1.1, and 1.8 mm into a cylindrical cell of fixed diameter ($D=2.5$ cm), the packings is effective rescaled with diameters of $D\rightarrow D/d=50$, 22.7, and 13.9. Because the packing is much taller than it is wide, D/d is the smallest dimension and should be principally responsible for finite-size effects.

Figure 15 plots $v(\Gamma_0)$ for the three D/d studied, obtained using identical experimental protocols. Aside from an overall shift to larger v (lower ρ), the $v(\Gamma_0)$ curve for small D/d is not very different from that for large D/d. The reversible branch of $v(\Gamma_0)$ is slightly less steep, and the branch point Γ^* is less clearly defined, but overall, no drastic changes are apparent.

The differences stand out far more clearly when we compare the $\tilde{\chi}_v(\Gamma_0)$ for different values of D/d. As shown in Fig. 16, when tapping is either very strong or very weak, $\tilde{\chi}_v(\Gamma_0)$ is basically independent of system size, behaving as expected of an intensive quantity. But for intermediate Γ_0, where $\tilde{\chi}_v(\Gamma_0)$ has its broad peak, finite-size effects show up as a systematic suppression of the volumetric response for smaller systems. Thus, for these intermediate values of Γ_0, the dynamics of large systems are more sensitive, and responds more strongly to small variations in external driving.

Figure 17 compares the spectrum $\tilde{\chi}_v(f)$ obtained at fixed Γ_0 for the different system sizes. When strongly tapped, the spectrum of $\tilde{\chi}_v$ is essentially the same for all D/d [Fig. 17(a)], consistent with the Γ_0-domain observation that finite-size effects are absent in the strongly driven regime. As Γ_0 is lowered, the spectral peak in χ_v'' is increasingly suppressed for small systems. The suppression is asymmetric: the low-frequency wing of the spectral peak is more strongly suppressed than the high-frequency wing, so that for smaller D/d, the spectral peak is located at a higher frequency [Figs. 17(b) and 17(c)]. At still smaller values of Γ_0, while the spectral peak of a small system remains strongly suppressed, its low-frequency wing also decays slower, so that at the lowest frequencies measured, χ_v'' for small systems is moderately enhanced relative to that of large D/d [Figs. 17(d) and 17(e)]. Finally, for very weak tapping, the spectrum of $\tilde{\chi}_v$ become once again essentially the same for all system sizes [Fig. 17(f)].

While finite system size manifests itself in $v(\Gamma_0)$ mostly as a uniform shift to lower density, its effects on $\tilde{\chi}_v$ exhibit nontrivial variations with respect to Γ_0 and f. Clearly, the system size can have a strong and complex effect on the dynamics of granular compaction.

B. Extrinsic and intrinsic length scales

The surface-to-volume ratio of a cylindrical packing scales with the diameter as $(D/d)^{-1}$. Thus for small systems, dynamical processes that take place near the boundary will have proportionally stronger influence on overall behavior. The wall restricts not only the motion of particles near the boundary, but also how they can pack, particularly if D/d is small and the boundary curvature proportionally large. The hindrance to efficient packing due to boundary curvature is likely responsible for the reduced packing density of small systems.

At small tapping amplitudes $\Gamma_0\leq 7$, I observe that the particles adjacent to the cell wall arrange into an ordered triangular layer that is nearly immobile. The larger surface-to-volume ratio of small systems means a greater proportion of total particles are semi-immobilized by the wall-induced ordering. This may explain the excess response of small systems at very low frequencies and weak tapping [Figs. 17(d) and 17(e)]: these are contributed by slow particle rearrangements in the ordered boundary layer. But it does not explain

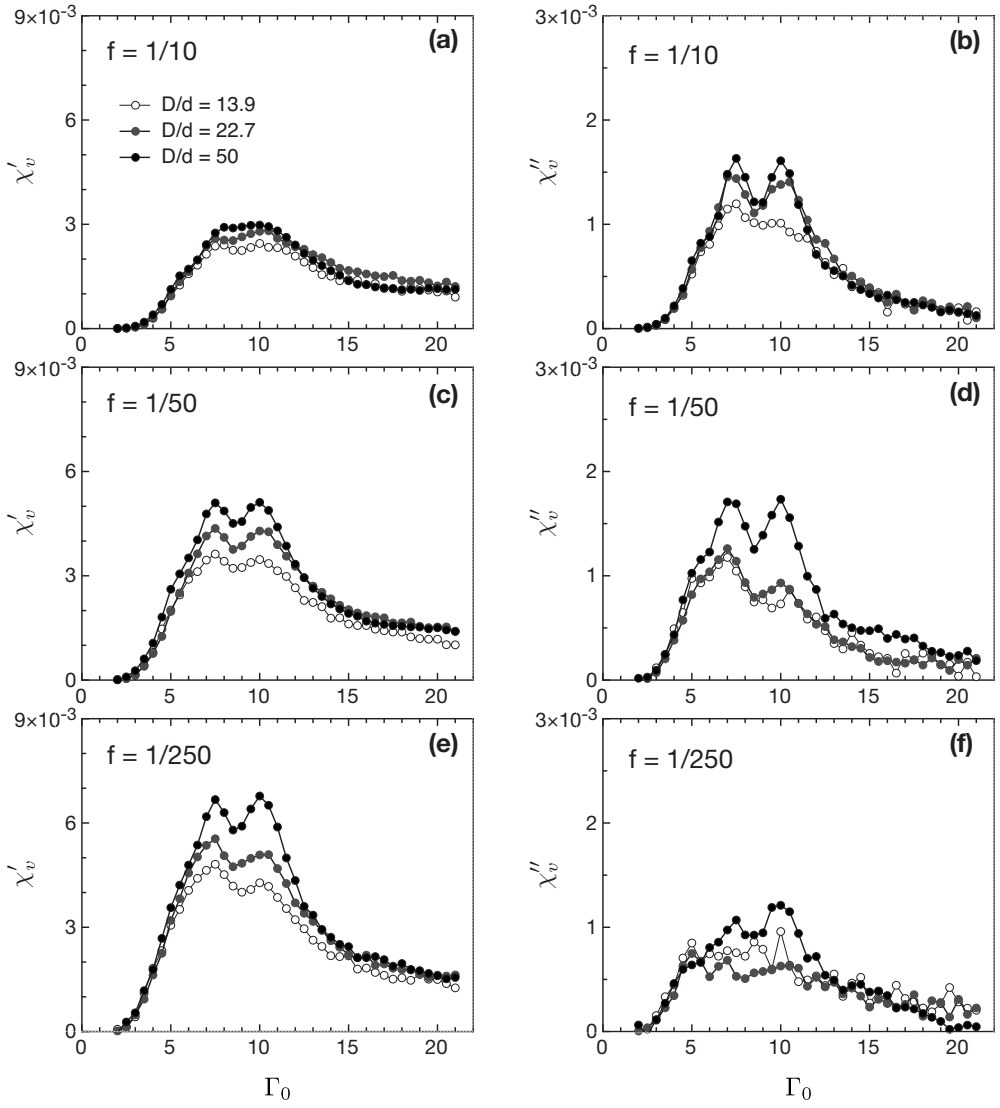

FIG. 16. The effect of finite size on the Γ_0-dependence of $\tilde{\chi}_v$ measured at frequencies of (a, b) $f=10^{-1}$ taps^{-1}, (c, d) $f=50^{-1}$ taps^{-1}, and (e, f) $f=250^{-1}$ taps^{-1}. The systems sizes measured are $D/d=50$, 22.7, and 13.9.

the asymmetric suppression of the spectral peak in $\chi''_v(f)$.

Suppose the rare, low-frequency processes that give granular compaction its glassy character arise from the collective particles rearrangements with a dynamic correlation length ξ. Then the asymmetric suppression of low-frequency volumetric response in small systems may be understood as the truncation of large-scale rearrangements by finite system size. Such a scenario is consonant with the usual intuition that low-f responses are constituted by large-scale rearrangement of many particles, while high-f responses arise from localized rearrangements. In this case, the frequency spectrum can be mapped onto a spectrum of correlation lengths, $f \rightarrow \xi(f)$, characterizing collective rearrangements.

Assuming that the low-f roll-off in the peak of $\chi''_v(f)$ takes place at $f=f_D$, corresponding to $\xi(f_D)=D/d$, then the typical dynamical correlation length ξ_p, corresponding to the peak frequency f_p, must be smaller than D/d. Using this crude bound, for $D/d=50$, ξ_p should not be more than ~ 20 particle diameters. Furthermore, as finite-size effects are apparent only for intermediate Γ_0, ξ_p must have a nonmonotonic variation with Γ_0; it should be smaller than the smallest D/d (=13.9) when the tapping is either very strong and very gentle, while reaching maximum size at some intermediate value of Γ_0.

C. Comparison with glasses

The suggestion that particle rearrangements during granular compaction may be collective in consonant with what we know about dynamic correlations in glasses and driven granular systems. Simulations of glass-forming liquids have found stringlike clusters of mobile particles that rearrange collectively, whose typical length scale grows from ~ 5 to ~ 20 particle diameters approaching T_g [53,54]. Studies of glass-forming liquids using nanoconfinement [55,56], specific heat spectroscopy [57], multipoint susceptibilities [58], and nuclear magnetic resonance [59] all point indirectly toward growing dynamic correlations on the scale of tens of

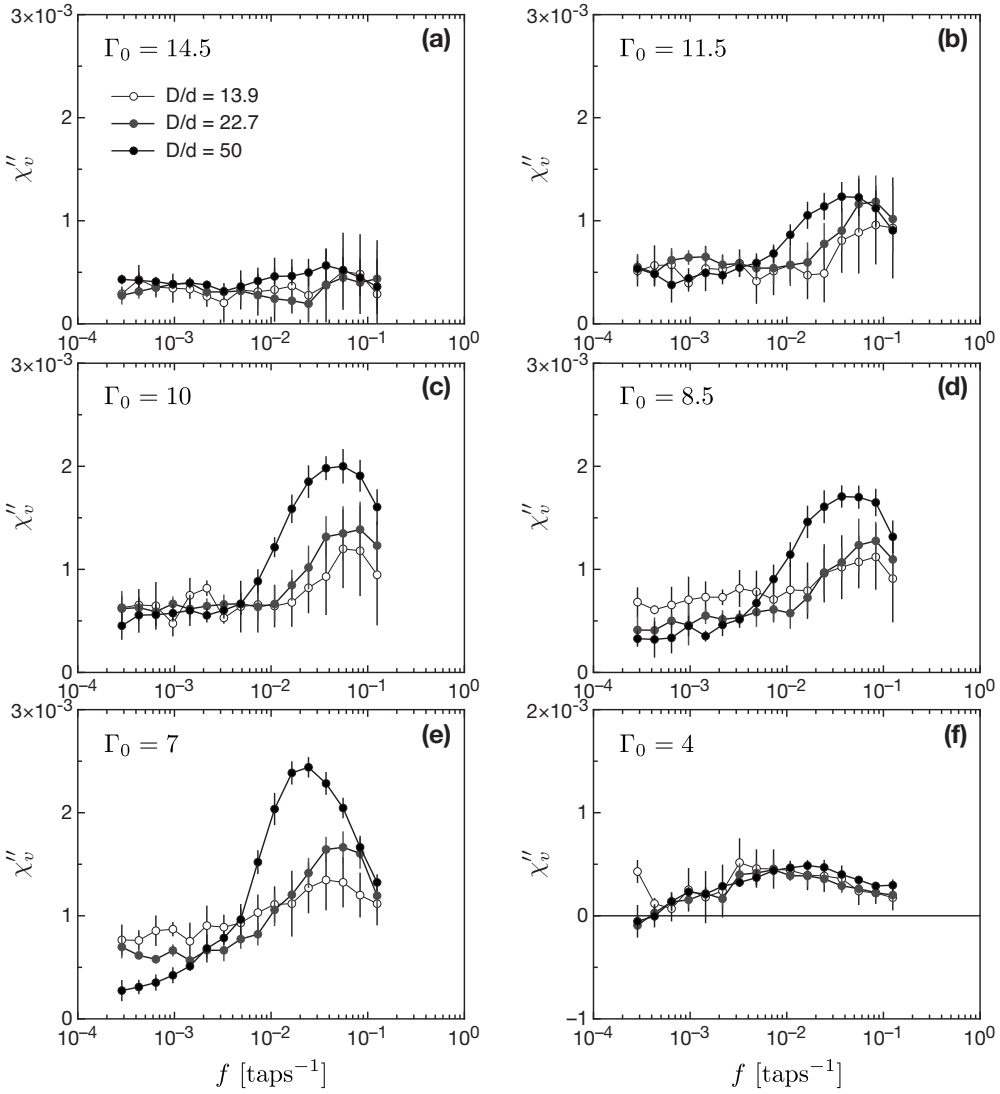

FIG. 17. The effect of finite size on $\chi_v''(f)$, the imaginary part of $\tilde{\chi}_v$ spectrum, measured at (a) Γ_0=14.5, (b) Γ_0=11.5, (c) Γ_0=10, (d) Γ_0=8.5, (e) Γ_0=7, and (f) Γ_0=4.

molecular diameters as $T \rightarrow T_g$. Collective rearrangements have been observed in colloidal glasses where the glass transition is controlled by the colloidal volume fraction ϕ. Approaching the glass transition $\phi = \phi_g$, dynamically correlated clusters grow in size from a few to a few tens of particle diameters [60,61]. In granular systems, 2D compaction experiments have observed slowly evolving hexagonal domains [62]. Stringlike clusters of dynamically correlated particles, ~10 particle diameters in size, have been observed in 2D granular beds fluidized by air flow; these grow larger as air flow is reduced [63]. Self-organized clusters also show up in 2D packings of slowly swelling tapioca pearls; as the system approaches jamming, the clusters grow in size [64].

VI. DISCUSSION AND OUTLOOK

A. Glassy state of granular compaction

In this paper, I have described using a volumetric spectroscopy to study the glassy dynamics of tapping-induced granular compaction. Despite some qualitative similarities, the volumetric susceptibility $\tilde{\chi}_v$ differs in important ways from its dielectric and magnetic counterparts in structural and spin glasses. Most notably, $\tilde{\chi}_v$ does not appear to be very glassy: it exhibits minimal aging, and its spectrum gives no indication of a rapidly growing time scale as external driving is turned down.

Simulations show that the dynamic specific heat $\tilde{c}$ in standard 2D spin-glass models behaves strikingly similar to $\tilde{\chi}_v$. I hypothesize the features of $\tilde{\chi}_v$ are not distinctive to granular compaction, but may be generic to the specific heat of purely configurational glasses. This hypothesis is supported by an effective FDT relationship between $\tilde{\chi}_v$ and volume fluctuations.

If $\tilde{\chi}_v$ can be taken as a specific heat, then it should contain contributions from all dynamical processes, including those responsible for glassy behavior. That a diverging time scale cannot be discerned from the spectrum of $\tilde{\chi}_v$ suggests glassy behavior is controlled by statistically rare events in the low-frequency wing. As Γ_0 (or T) is reduced, these glassy pro-

cesses become rapidly separated in time scale from typical system dynamics, leading to broken ergodicity and glassy behavior.

Finite-size effects in $\tilde{\chi}_v$ suggest that the glassy dynamics in granular compaction are due to collective particle rearrangements with a typical correlation length $\xi < 20$ particle diameters. This appear to point toward a "droplet" picture of the glassy state in granular compaction. In this picture, the glass is a mosaic composed of small domains (droplets) drawn from a family of disordered equilibrium thermodynamic phases; the surface energy of the droplets scales weakly with droplet size, so that droplet growth is slow and no droplet can dominate the system [65,66]. While most of the dynamical processes in the glass come from equilibrium droplet fluctuations, the droplets can also grow or shrink via rare activated events which are responsible for glassy dynamics. This suggests glassy processes will be truncated in small systems with dimensions comparable to typical droplet size. My results suggest perhaps a similar droplet picture may describe granular compaction as well.

B. Connection to jamming

Frictionless hard spheres have a well-defined jamming point J (where $\rho = \rho_{\mathrm{rcp}}$) that exhibits scaling properties marking it as an unconventional critical point [67–69]. Being a $T=0$ phenomenon, the jamming transition does not contain any dynamics. But evidences from experiments and simulations suggest that the critical properties of point J can influence dynamics at finite T, where point J is not directly accessible, and be felt in a modified form as the glass transition [70,71].

In granular compaction, the ideal transition between jammed and unjammed states at point J cannot be explored, since any packings produced experimentally is automatically jammed. In the presence of friction, instead of a single jamming point, there is a large configuration space of jammed states, with densities ranging from random loose packing at $\rho_{\mathrm{rlp}} \approx 0.55$ up to $\rho_{\mathrm{rcp}} \approx 0.64$. Tapping provides the dynamics for the system to explore this configuration space, with point J being an idealized limit.

If point J can influence dynamics at finite T, it may also influence the finite-friction dynamics of granular compaction. I suggest that the transition between liquid and glass, and the transition between steady-state and glassy dynamics in granular compaction, may be thought as two aspects of the same idealized jamming transition, manifested nonideally at finite T and finite friction, respectively. This may be why similar dynamical manifestations, such as collective rearrangements on the scales of few tens of particles, are found in both glasses and externally driven granular packings.

In jamming, point J marks the divergence of a dynamical correlation length associated with vibrational modes of the system [68,72,73]. This divergence does not survive away from zero temperature and zero friction, but it may leave behind vestigial signatures. For granular compaction, it will be illuminating to study the volumetric response of ever larger systems to see when finite-size effects disappear completely. This should give an upper critical length for collective rearrangements during compaction. It will be interesting if this upper critical length turns out to be very large. Since granular compaction is arguably closer to the ideal $T=0$ jamming transition than colloidal glasses or glass-forming liquids, it may be that a diverging length scale associated with point J will leave a larger vestige in granular compaction.

C. Kinetic versus configurational "glasses"

In glass-forming liquids, the dynamic specific heat shows a rapidly growing characteristic time as T is reduced. However, this stereotypical glassy signature is apparently absent in the dynamic specific heat of model spin glasses. Since the specific heat receives contributions from all dynamical processes, this suggests that the glassy dynamics of structural glass-formers is due to an overall dynamical slowing-down, while that of spin glasses is controlled by a statistically rare subset of low-f processes which diverge from typical dynamics.

Does this mean the glass transition in liquids with kinetic degrees of freedom, is qualitatively different from the transition in purely configurational systems such as spin glasses? Interestingly, granular compaction, taken as a "glassy" system whose volumetric susceptibility χ_v is analogous to the specific heat, appears to bridge the difference: structurally it looks like a glassy solid, but its dynamics is closer to that of a spin glass. While experimental and simulation results for the dynamic specific heat are available for several glassy-forming liquids, no similar results are available for spin glasses from either simulations or experiment (admittedly, the latter is difficult to realize). Thus, definite comparisons between kinetic and configurational glasses cannot yet be made. Here, granular compaction may prove to be an useful experimental system. By applying volumetric spectroscopy to continuously driven granular packings, where kinetic energy is important, we can ask if $\tilde{\chi}_v$ now behaves more like the dynamic specific heat of liquids. Hints that this is the case comes from rotational spectroscopy on fluidized granular packings that do find a growing time scale with decreasing external driving [74–76]. The limiting state of granular compaction, whether discretely or continuously driven, should be the same. If granular compaction can exhibit both liquidlike and spin-glass-like dynamics on the way to that limit, depending on how it is driven, it would suggest that the glassy transition in kinetic and configurational systems are fundamental similar.

I will conclude with this remark: throughout this paper, I have made operational analogies between granular compaction under external driving, and glassy systems at finite temperatures, without offering any first-principle justifications. However, recall that for all but the simplest thermal systems, the basic concepts of equilibrium statistical mechanics cannot be justified except by their utility in helping us understanding experimental results. Apart from what it tells us about granular compaction or glassy dynamics, a principal value of the experiments described here is as tests for the usefulness of a statistical mechanics description of granular matter.

ACKNOWLEDGMENTS

I am greatly indebted to Sidney Nagel for his advice, criticism, and support through the course of my work. I have also benefited from discussions with Tom Witten, Dan Silevitch, Sue Coppersmith, Bob Leheny, Heinrich Jaeger, Simon Swordy, and Scott Wakely. Special acknowledgment is due to Xiang Cheng not only for many fruitful discussions, but also for his technical assistance. This work is supported by NSF MRSEC under Grant No. DMR-0820054, NSF under Grant No. DMR-0652269, and DOE under Grant No. DE-FG02-03ER46088.

[1] T. Aste and D. Weaire, *The Pursuit of Perfect Packing*, 2nd ed. (Taylor and Francis, New York, 2008).
[2] H. M. Jaeger and S. R. Nagel, Science **255**, 1523 (1992).
[3] G. D. Scott, Nature (London) **188**, 908 (1960).
[4] J. D. Bernal, Nature (London) **183**, 141 (1959).
[5] J. D. Bernal, Nature (London) **185**, 68 (1960).
[6] J. D. Bernal, Proc. R. Soc. London, Ser. A **280**, 299 (1964).
[7] G. D. Scott, Nature (London) **194**, 956 (1962).
[8] J. L. Finney, Proc. R. Soc. London, Ser. A **319**, 479 (1970).
[9] J. C. Maxwell, Philos. Mag. Ser. 4 **182**, 294 (1864).
[10] J. L. Finney, Nature (London) **266**, 309 (1977).
[11] R. W. Cahn, Contemp. Phys. **21**, 43 (1980).
[12] R. Zallen, *The Physics of Amorphous Solids* (Wiley-Interscience, New York, 1998).
[13] A. J. Liu and S. R. Nagel, Nature (London) **396**, 21 (1998).
[14] L.-N. Zou, X. Cheng, M. L. Rivers, H. M. Jager, and S. R. Nagel, Science **326**, 408 (2009).
[15] L. Lopatina, C. Olson Reichhardt, and C. Reichhardt, e-print arXiv:0912.1874.
[16] M. D. Ediger, C. A. Angell, and S. R. Nagel, J. Phys. Chem. **100**, 13200 (1996).
[17] K. Binder and A. P. Young, Rev. Mod. Phys. **58**, 801 (1986).
[18] F. Ritort and P. Sollich, Adv. Phys. **52**, 219 (2003).
[19] J. B. Knight, C. G. Fandrich, C. N. Lau, H. M. Jaeger, and S. R. Nagel, Phys. Rev. E **51**, 3957 (1995).
[20] E. R. Nowak, J. Knight, M. Povinelli, H. M. Jaeger, and S. R. Nagel, Powder Technol. **94**, 79 (1997).
[21] P. Philippe and D. Bideau, EPL **60**, 677 (2002).
[22] E. R. Nowak, J. B. Knight, E. Ben-Naim, H. M. Jaeger, and S. R. Nagel, Phys. Rev. E **57**, 1971 (1998).
[23] C. Josserand, A. V. Tkachenko, D. M. Mueth, and H. M. Jaeger, Phys. Rev. Lett. **85**, 3632 (2000).
[24] P. Richard, M. Nicodemi, R. Delannay, P. Ribière, and Daniel Bideau, Nature Mater. **4**, 121 (2005).
[25] P. Ribière, P. Richard, P. Philippe, D. Bideau, and R. Delannay, Eur. Phys. J. E **22**, 249 (2007).
[26] H. K. Pak, E. Van Doorn, and R. P. Behringer, Phys. Rev. Lett. **74**, 4643 (1995).
[27] N. Menon, K. P. O'Brien, P. K. Dixon, L. Wu, S. R. Nagel, B. D. Williams, and J. P. Carini, J. Non-Cryst. Solids **141**, 61 (1992).
[28] D. H. Reich, B. Ellman, J. Yang, T. F. Rosenbaum, G. Aeppli, and D. P. Belanger, Phys. Rev. B **42**, 4631 (1990).
[29] J. A. Quilliam, S. Meng, C. G. A. Mugford, and J. B. Kycia, Phys. Rev. Lett. **101**, 187204 (2008).
[30] C. A. M. Mulder, A. J. van Duyneveldt, and J. A. Mydosh, Phys. Rev. B **23**, 1384 (1981).
[31] C. A. M. Mulder, A. J. van Duyneveldt, and J. A. Mydosh, Phys. Rev. B **25**, 515 (1982).
[32] G. F. Zhou and H. Bakker, Phys. Rev. Lett. **72**, 2290 (1994).
[33] J.-O. Andersson, T. Jonsson, and J. Mattsson, Phys. Rev. B **54**, 9912 (1996).
[34] R. L. Leheny and S. R. Nagel, Phys. Rev. B **57**, 5154 (1998).
[35] E. Vincent, J. P. Bouchaud, J. Hammann, and F. Lefloch, Philos. Mag. B **71**, 489 (1995).
[36] S. Havriliak and S. Negami, J. Polymer Sci. Part C **14**, 99 (1966).
[37] S. F. Edwards and R. B. S. Oakeshott, Physica A **157**, 1080 (1989).
[38] S. F. Edwards and D. V. Grinev, Phys. Rev. E **58**, 4758 (1998).
[39] J. P. Sethna, *Statistical Mechanics: Entropy, Order Parameters, and Complexity* (Oxford University Press, New York, 2009).
[40] J. K. Nielsen and J. C. Dyre, Phys. Rev. B **54**, 15754 (1996).
[41] Th. M. Nieuwenhuizen, Phys. Rev. Lett. **80**, 5580 (1998).
[42] N. O. Birge and S. R. Nagel, Phys. Rev. Lett. **54**, 2674 (1985).
[43] N. O. Birge, Phys. Rev. B **34**, 1631 (1986).
[44] P. K. Dixon and S. R. Nagel, Phys. Rev. Lett. **61**, 341 (1988).
[45] P. K. Dixon, Phys. Rev. B **42**, 8179 (1990).
[46] P. Scheidler, W. Kob, A. Latz, J. Horbach, and K. Binder, Phys. Rev. B **63**, 104204 (2001).
[47] K. A. Mirza and J. W. Loram, J. Phys. F: Met. Phys. **15**, 439 (1985).
[48] S. Nagata, R. R. Galazka, D. P. Mullin, H. Akbarzadeh, G. D. Khattak, J. K. Furdyna, and P. H. Keesom, Phys. Rev. B **22**, 3331 (1980).
[49] Y. Takano, A. Arai, Y. Takahashi, K. Takase, and K. Sekizawa, J. Appl. Phys. **93**, 8197 (2003).
[50] M. Cieplak and G. Szamel, Phys. Rev. B **37**, 1790 (1988).
[51] R. G. Palmer, Adv. Phys. **31**, 669 (1982).
[52] J. P. Bouchaud, J. Phys. I (France) **2**, 1705 (1992).
[53] C. Donati, J. F. Douglas, W. Kob, S. J. Plimpton, P. H. Poole, and S. C. Glotzer, Phys. Rev. Lett. **80**, 2338 (1998).
[54] C. Donati, S. C. Glotzer, P. H. Poole, W. Kob, and S. J. Plimpton, Phys. Rev. E **60**, 3107 (1999).
[55] M. Arndt, R. Stannarius, H. Groothues, E. Hempel, and F. Kremer, Phys. Rev. Lett. **79**, 2077 (1997).
[56] C. Alba-Simionesco, G. Dosseh, E. Dumont, B. Frick, B. Geil, D. Morineau, V. Teboul, and Y. Xia, Eur. Phys. J. E **12**, 19 (2003).
[57] E. Donth, H. Huth, and M. Beiner, J. Phys.: Condens. Matter **13**, L451 (2001).
[58] L. Berthier, G. Biroli, J.-P. Bouchaud, L. Cipelletti, D. El Masri, D. L'Hôte, F. Ladieu, and M. Pierno, Science **310**, 1797 (2005).
[59] S. A. Reinsberg, X. H. Qiu, M. Wilhelm, H. W. Spiess, and M. D. Ediger, J. Chem. Phys. **114**, 7299 (2001).
[60] E. R. Weeks, J. C. Cocker, A. C. Levitt, A. Schofield, and D.

A. Weitz, Science **287**, 627 (2000).
[61] B. Cui, B. Lin, and S. A. Rice, J. Chem. Phys. **114**, 9142 (2001).
[62] G. Lumay and N. Vandewalle, Phys. Rev. Lett. **95**, 028002 (2005).
[63] A. S. Keys, A. R. Abate, S. C. Glotzer, and D. J. Durian, Nat. Phys. **3**, 260 (2007).
[64] X. Cheng, Phys. Rev. E **81**, 031301 (2010).
[65] V. Lubchenko and P. G. Wolynes, J. Chem. Phys. **121**, 2852 (2004).
[66] V. Lubchenko and P. G. Wolynes, Annu. Rev. Phys. Chem. **58**, 235 (2007).
[67] C. S. O'Hern, L. E. Silbert, A. J. Liu, and S. R. Nagel, Phys. Rev. E **68**, 011306 (2003).
[68] L. E. Silbert, A. J. Liu, and S. R. Nagel, Phys. Rev. Lett. **95**, 098301 (2005).
[69] L. E. Silbert, A. J. Liu, and S. R. Nagel, Phys. Rev. E **73**, 041304 (2006).
[70] Z. Zhang *et al.*, Nature (London) **459**, 230 (2009).
[71] N. Xu, T. K. Haxton, A. J. Liu, and S. R. Nagel, Phys. Rev. Lett. **103**, 245701 (2009).
[72] M. Wyart, S. R. Nagel, and T. A. Witten, EPL **72**, 486 (2005).
[73] M. Wyart, L. E. Silbert, S. R. Nagel, and T. A. Witten, Phys. Rev. E **72**, 051306 (2005).
[74] G. D'Anna and G. Gremaud, EPL **54**, 599 (2001).
[75] G. D'Anna and G. Gremaud, Nature (London) **413**, 407 (2001).
[76] G. D'Anna, P. Mayor, A. Barrat, V. Loreto, and Franco Nori, Nature (London) **424**, 90 (2003).